Neuron
Article

Nitration of Tyrosine 10 Critically Enhances Amyloid β Aggregation and Plaque Formation

Markus P. Kummer,[1] Michael Hermes,[1] Andrea Delekarte,[2] Thea Hammerschmidt,[1,3] Sathish Kumar,[4] Dick Terwel,[1] Jochen Walter,[4] Hans-Christian Pape,[3] Simone König,[5] Sigrun Roeber,[6] Frank Jessen,[7,8] Thomas Klockgether,[1,8] Martin Korte,[2] and Michael T. Heneka[1,8,*]
[1]Clinical Neuroscience Unit, Department of Neurology, University of Bonn, Sigmund-Freud-Strasse 25, 53127 Bonn, Germany
[2]Division of Cellular Neurobiology, Zoological Institute, TU Braunschweig, 38106 Braunschweig, Germany
[3]Institut for Physiology I, University of Münster, Robert-Koch-Strasse 27a, 48149 Münster, Germany
[4]Molecular Neurology Group, Department of Neurology, University of Bonn, Sigmund-Freud-Strasse 25, 53127 Bonn, Germany
[5]Integrated Functional Genomics, Interdisciplinary Center for Clinical Research Münster, Röntgenstrasse 21, 48149 Münster, Germany
[6]Institute for Neuropathology, Ludwig-Maximilian University, Feodor-Lynen-Strasse 23, 81377 München, Germany
[7]Department of Psychiatry, University of Bonn, Sigmund-Freud-Strasse 25, 53127 Bonn, Germany
[8]German Center for Neurodegenerative Diseases, Ludwig-Erhard-Allee 2, 53175 Bonn, Germany
*Correspondence: michael.heneka@ukb.uni-bonn.de
DOI 10.1016/j.neuron.2011.07.001

SUMMARY

Part of the inflammatory response in Alzheimer's disease (AD) is the upregulation of the inducible nitric oxide synthase (NOS2) resulting in increased NO production. NO contributes to cell signaling by inducing posttranslational protein modifications. Under pathological conditions there is a shift from the signal transducing actions to the formation of protein tyrosine nitration by secondary products like peroxynitrite and nitrogen dioxide. We identified amyloid β (Aβ) as an NO target, which is nitrated at tyrosine 10 (3NTyr^{10}-Aβ). Nitration of Aβ accelerated its aggregation and was detected in the core of Aβ plaques of APP/PS1 mice and AD brains. NOS2 deficiency or oral treatment with the NOS2 inhibitor L-NIL strongly decreased 3NTyr^{10}-Aβ, overall Aβ deposition and cognitive dysfunction in APP/PS1 mice. Further, injection of 3NTyr^{10}-Aβ into the brain of young APP/PS1 mice induced β-amyloidosis. This suggests a disease modifying role for NOS2 in AD and therefore represents a potential therapeutic target.

INTRODUCTION

Alzheimer's disease (AD) is clinically characterized by progressive memory loss and decline of cognitive functions. Besides the classical histopathological hallmarks, extracellular amyloid β (Aβ) deposition and neurofibrillary tangles of tau protein, neuroinflammation has been established as a major component (Querfurth and LaFerla, 2010). This inflammatory response includes the activation of astrocytes and microglial cells localized to senile plaques and the release of biochemical markers, including cytokines, chemokines, and nitric oxide, that are found to be increased in the brains of patients with AD (Glass et al., 2010). While the generation of Aβ peptides from the amyloid precursor protein as well as their propensity to aggregate into β-cross sheet fibrils has been well characterized (Querfurth and LaFerla, 2010), the mutual interactions between neuroinflammation, Aβ formation and deposition remain to be elucidated.

While neuronal nitric oxide synthase 1 (NOS1) is constitutively expressed in a subset of neurons, AD-associated inflammation can increase NOS1 and the inducible nitric oxide synthase (NOS2) expression in neurons (Fernández-Vizarra et al., 2004; Vodovotz et al., 1996; Heneka et al., 2001) along with the upregulation of NOS2 in microglia and astrocytes (Fernández-Vizarra et al., 2004; Vodovotz et al., 1996; Heneka et al., 2001). NOS2 catalyzes the generation of NO, which has been implicated in impairment of mitochondrial respiration (Beal, 2000), synaptic failure, and neuronal cell death (Nakamura and Lipton, 2009) during neurodegeneration. One of the fingerprints of NO is tyrosine nitration, a posttranslational protein modification, resulting in the formation of 3′-nitrotyrosine residues (Radi, 2004) that can induce structural changes leading to protein aggregation (Radi, 2004). Indeed, AD lesions reveal the pathological pattern of nitrosative injury (Fernández-Vizarra et al., 2004; Castegna et al., 2003; Colton et al., 2008; Lüth et al., 2002), prominently in brain areas that are affected in AD (Hensley et al., 1998).

So far, it is unknown why the Aβ peptide, present at high levels under nonpathological conditions in humans, under certain circumstances starts to multimerize leading to the formation of Aβ oligomers and further to high molecular weight fibrils and plaques. In murine models of AD, the overexpression of the human amyloid precursor protein (APP) results in the formation of plaque pathology, whereas wild-type mice and rats do not innately develop amyloid deposits with age (Shivers et al., 1988), even after overexpression of endogenous APP (Jankowsky et al., 2007).

APP is a highly conserved transmembrane protein with only 4% difference in amino acid between human, monkey, mouse, and rat sequence. Three of these differences (R5 → G, Y10 → F, and H13 → R) are localized to the Aβ domain (Figure 1A), giving rise to speculations about the importance of these changes for amyloid deposition. Surprisingly, synthetic peptides

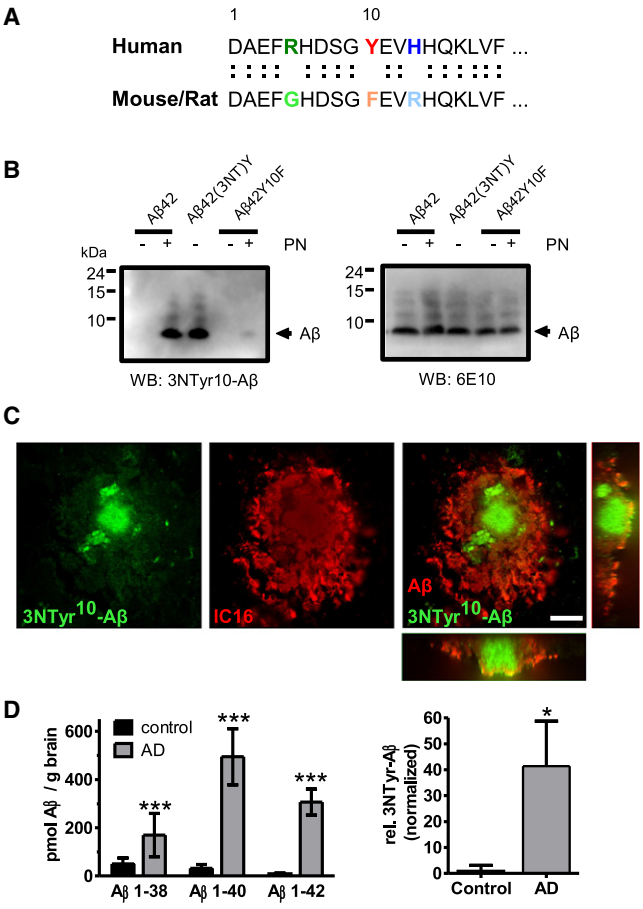

Figure 1. Detection of Aβ Nitrated at Tyrosine 10 in AD Brains

(A) Amino acid alignment of human, mouse/rat Aβ. Differences are colored.

(B) 3NTyr^{10}-Aβ antiserum specifically detects nitrated Aβ. Aβ$_{1-42}$ (Aβ42) and the Aβ$_{1-42}$Y10F mutant (Aβ42Y10F) were incubated in the absence and presence of peroxynitrite and immunoblotted using 3NTyr^{10}-Aβ antiserum. In addition, synthetically nitrated Aβ$_{1-42}$ (Aβ42(3NT)Y) was used as a control. Samples were reprobed using antibody 6E10.

(C) Immunohistochemical detection of nitrated Aβ in human AD tissue using IC16 against Aβ and 3NTyr^{10}-Aβ antiserum by confocal microscopy. Nitrated Aβ was detected in the core of amyloid plaques (bar = 20 μm).

D) Relative quantification of Aβ$_{1-38}$, 1-40, 1-42 and 3NTyr^{10}-Aβ in the SDS fraction of AD brains and controls measured by sandwich ELISA (n = 5 for control and n = 8 for AD ± SEM, Student-s t test, *p < 0.05, ***p < 0.001).

See also Figure S1.

containing these mutations do not differ in the propensity to form high molecular weight aggregates in vitro (Wahle et al., 2006). An alternative explanation could be that posttranslational modifications of the Aβ peptide are essential to initiate its aggregation, as it has been shown for pyroglutamate-modified Aβ (Querfurth and LaFerla, 2010; He and Barrow, 1999). Of note, induction of aggregation by NO modifications has been reported for other disease-relevant proteins (Nakamura and Lipton, 2009). With regards to the amino acid sequence of Aβ, the tyrosine at position 10 is a potential target for protein nitration.

Since there is so far no mechanistic explanation of how expression of NOS2 and the subsequent production of NO and its reaction products modulate the progression of AD, we speculated that nitration of Aβ might contribute to AD pathology.

We report here the presence of Aβ nitrated at tyrosine 10 in AD as well as in AD mouse models. This modification accelerated the deposition of human Aβ. We further find that Aβ burden and deficits in memory formation were ameliorated in APP/PS1 NOS2 (−/−) mice or by pharmacological treatment with a NOS2 inhibitor. Finally, nitrated Aβ was able to induce β-amyloidosis in APP/PS1 mice. These results underline the importance of this posttranslational modification as a potential therapeutic target.

RESULTS

Detection of Nitrated Aβ in AD Tissue

Since tyrosine 10 represents a potential nitration side (Figure 1A), we tested the availability of this amino acid for this posttranslational modification in vitro. Performing mass spectrometry analysis after tryptic digestion of Aβ$_{1-42}$ that was either nitrated using peroxynitrite or the NO-donor Sin-1, we observed the described fragmentation pattern of a nitrated peptide (Petersson et al., 2001). This pattern was missing using Aβ$_{1-42}$ bearing a tyrosine to alanine mutation (see Figure S1 available online), suggesting that tyrosine 10 is a potential nitration target in vitro.

To detect Aβ nitrated at tyrosine 10 (3NTyr^{10}-Aβ), we generated an antiserum specifically recognizing this epitope (3NTyr^{10}-Aβ antiserum). This antiserum showed strong immunoreactivity against peroxynitrite-treated Aβ$_{1-42}$ peptide or synthetically-nitrated Aβ$_{1-42}$ (Aβ42(3NT)Y), which was absent in case of the untreated peptide (Figure 1B). We observed a very low amount of reactivity when treating Aβ$_{1-42}$Y10F mutant peptide with peroxynitrite. This might be caused by the conversion of phenylalanine to tyrosine by hydroxyl radicals generated during the decomposition of peroxynitrite (Ferger et al., 2001). In accordance with this, there was no reactivity toward Aβ$_{1-42}$ bearing a Y10A mutation after incubation with peroxynitrite (Figure S1). Using this antiserum, we were able to detect 3NTyr^{10}-Aβ in the supernatant of NOS2 overexpressing HEK293 cells after exogenous addition of non-aggregated Aβ, demonstrating that NOS2 is able to induce this posttranslational modification before Aβ deposits form (Figure S1).

Immunohistochemical analysis of AD and control brains by 3NTyr^{10}-Aβ antiserum revealed a lack of immunoreactivity in control brains, whereas in AD brain, the core of amyloid plaques was intensively labeled, as confirmed by IC16 double staining (Figure 1C). Measuring the relative amounts of 3NTyr^{10}-Aβ by sandwich ELISA in SDS-soluble fractions of human brain samples, we detected 3NTyr^{10}-Aβ in the SDS fraction of AD patients and only to very low amount in nondemented controls (Figure 1D). Further, the relative signal ratio of 3NTyr^{10}-Aβ between control and AD patients was comparable to that of Aβ$_{1-42}$ (Figure 1D). Of note, we failed to detect any 3NTyr^{10}-Aβ in human cerebrospinal fluid (CSF) of control, mild cognitive impaired, and AD patients underlining the insoluble properties of this species (Figure S1).

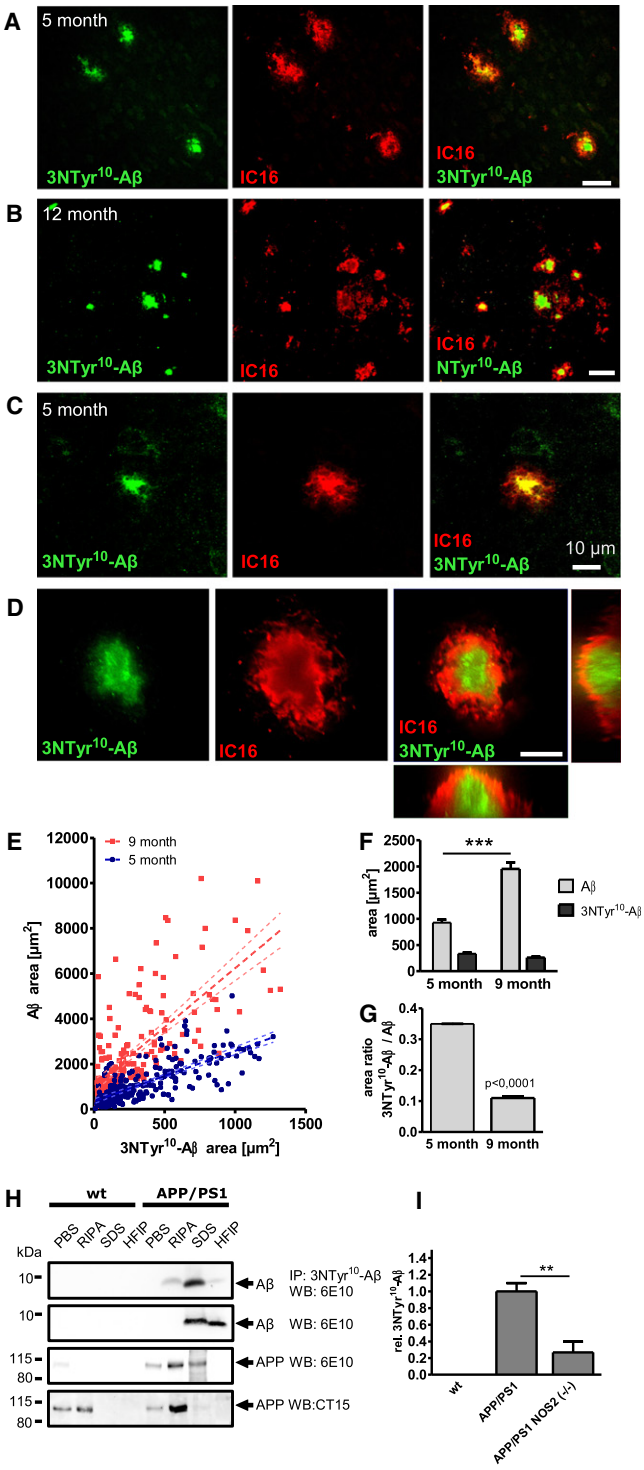

Figure 2. Nitrated Aβ Is Present in APP/PS1 Mice and Is Reduced after NOS2 Knockout

(A) Nitrated Aβ is already detectable in the cortex of 5-month-old APP/PS1 transgenic mice using antibody IC16 (Aβ) and 3NTyr^{10}-Aβ antiserum (bar = 50 μm).

(B) Detection of nitrated Aβ in 12-month-old APP/PS1 mice using antibody IC16 (Aβ) and 3NTyr^{10}-Aβ antiserum (bar = 50 μm).

(C) Nitrated Aβ are detectable in small plaques of around 10 μm in diameter (bar = 10 μm).

(D) Confocal 3D reconstruction of an Aβ plaque from a APP/PS1 mouse using IC16 and 3NTyr^{10}-Aβ (bar = 20 μm).

(E) Section from 5- and 9-month-old APP/PS1 mice were probed for 3NTyr^{10}-Aβ and Aβ using antibody IC16. Individual plaques were analyzed for 3NTyr^{10}-Aβ and Aβ area. (n = 4 mice, 275 plaques per group; lines, linear regression analysis; dashed lines, 95% confidence intervals, R^2 = 0.51 for 9 month group and R^2 = 0.57 for 5 month group).

(F) Statistical analysis of the average 3NTyr^{10}-Aβ and Aβ areas revealed that plaque growth increases Aβ area, whereas 3NTyr^{10}-Aβ area remains constant (mean ± SEM of n = 4 mice, 275 plaques per group analyzed, Student's t test).

(G) 3NTyr^{10}-Aβ/Aβ area ratios of individual plaques (mean ± SD of n = 4 mice, 275 plaques per group analyzed, Student's t test, ***p < 0.001).

(H) Brains of 12-month-old wild-type and APP/PS1 mice were sequentially extracted with PBS, RIPA, SDS, and finally with HFIP. Fractions were immunoprecipitated using 3NTyr^{10}-Aβ antiserum and immunoblotted using antibody 6E10. In addition, fractions were immunoblotted for Aβ and APP using antibodies 6E10 and CT15.

(I) 3NTyr^{10}-Aβ was measured by sandwich ELISA in SDS fractions of wild-type, APP/PS1, and APP/PS1 NOS2 (−/−) mice at 12 months of age (n = 4 ± SEM, Student's t test, **p < 0,01).

Nitration of Aβ Is Modulated by NOS2 in APP/PS1 Mice

Analysis of brain sections from 5- and 12-month-old APP/PS1 mice revealed a colocalization of antibody IC16 against Aβ with the 3NTyr^{10}-Aβ antiserum from beginning of plaque formation starting at 5 months of age in this AD mouse model (Figures 2A and 2B). This costaining was observed in all brain areas where amyloid plaques are formed. In addition, colocalization was observed independently of plaque size, since it was already detectable in tiny plaques of 10 μm diameter in 5-month-old animals (Figure 2C), suggesting that formation of 3NTyr^{10}-Aβ is an early event in plaque development. Similar to human AD brain, in APP/PS1 the 3NTyr^{10}-Aβ immunoreactivity was localized to the core of the plaque surrounded by IC16 immunoreactivity (Figure 2D).

Evaluation of individual Aβ plaque sizes by immunohistochemistry with antibody IC16 and the area of the 3NTyr^{10}-Aβ positive core of 5- and 9-month-old APP/PS1 mice revealed that there are no changes in the average 3NTyr^{10}-Aβ core size (Figures 2E and 2F), suggesting that the core, once formed, does not substantially increase in size any further. Nevertheless, we observed plaque growth between 5 and 9 months that was solely caused by accumulation of nonnitrated Aβ, as detected by IC16 immunoreactivity (Figures 2E and 2F). As a consequence, there was a highly significant drop in the 3NTyr^{10}-Aβ/Aβ ratio (Figure 2G).

In addition, we were able to immunoprecipitate 3NTyr^{10}-Aβ of brain homogenates sequentially extracted with PBS, RIPA, SDS, and HIFP using 3NTyr^{10}-Aβ antiserum. Using 6E10 as detection antibody, we were able to detect high amounts of nitrated Aβ in the SDS-soluble fraction and to smaller extent in the RIPA- and HFIP-soluble fractions of APP/PS1 mice (Figure 2H). Determining the relative amounts of 3NTyr^{10}-Aβ in SDS fractions of wild-type, APP/PS1, and APP/PS-1 NOS2 (−/−) animals by sandwich ELISA, we were unable to detect this species in wild-type mice, but in APP/PS1 mice. In turn, APP/PS1 mice lacking NOS2 (−/−) showed a 74% reduction of 3NTyr^{10}-Aβ (Figure 2I).

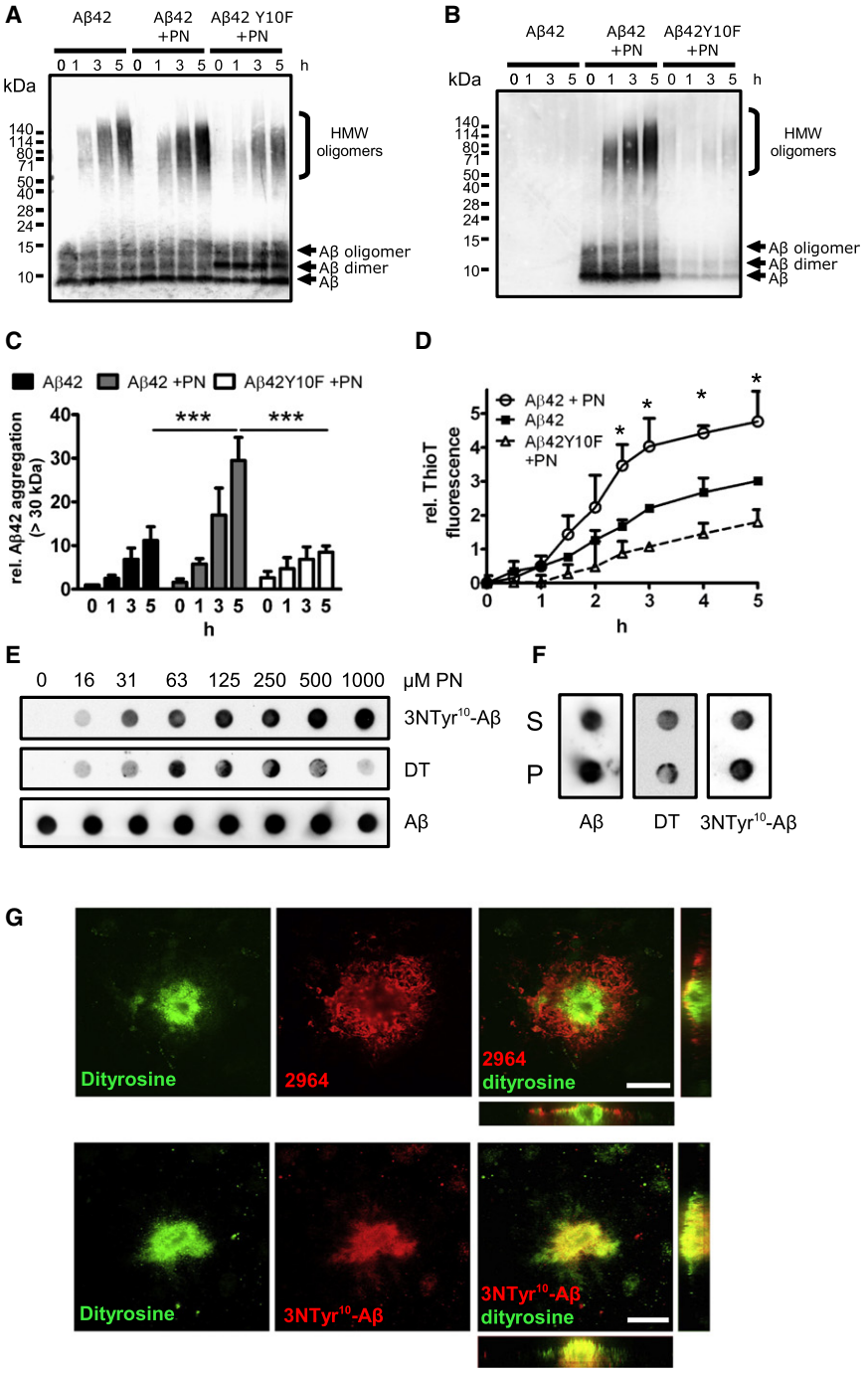

Figure 3. Nitration of Aβ at Tyrosine 10 Induces Its Aggregation

(A) Aggregation of synthetic $A\beta_{1-42}$ (Aβ42), nitrated $A\beta_{1-42}$ (Aβ42+PN), and nitrated $A\beta_{1-42}$Y10F (Aβ42Y10F + PN) was analyzed by western blot using antibody 6E10 (HMW oligomers, high molecular weight oligomers).

(B) Reprobing with 3NTyr^{10}-Aβ antiserum to detect Aβ nitration.

(C) Graphical evaluation of three independent experiments normalized to Aβ monomer (n = 3 ± SEM, two-way ANOVA, Bonferroni post test, ***$p < 0.001$).

(D) Thioflavin T aggregation assay of synthetic $A\beta_{1-42}$ (Aβ42), nitrated $A\beta_{1-42}$ (Aβ42+PN), and nitrated $A\beta_{1-42}$Y10F (n = 3 ± SEM, two-way ANOVA Aβ42 versus Aβ42 + PN, Bonferroni post test, *$p < 0.05$).

(E) Dot blot analysis of $A\beta_{1-42}$ (25 μM) after treatment with increasing concentration of peroxynitrite using antibody IC3 against dityrosine (DT), IC16 (Aβ), and 3NTyr^{10}-Aβ antiserum.

(F) Dot blot analysis of $A\beta_{1-42}$ (25 μM) for dityrosine (DT) after treatment with 250 μM of peroxynitrite, aggregation for 5 hr and subsequent centrifugation at 10000xg for 1 hr (S, supernatant; P, pellet).

(G) Confocal 3D reconstruction of an Aβ plaque from a 9-month-old APP/PS1 mouse using antibodies IC3 (dityrosine) and IC16 (Aβ) (bar = 20 μm) and using antibody IC3 (dityrosine) and 3NTyr^{10}-Aβ antiserum (bar = 20 μm).

See also Figure S2.

Nitration of Aβ at Tyrosine 10 Induces Its Aggregation

Since N-terminal modifications of Aβ have been shown to induce its aggregation, we speculated whether nitration of Aβ exerts a similar effect. Indeed, incubation of synthetic $A\beta_{1-42}$ with peroxynitrite or the NO donor Sin-1 resulted in increased generation of high molecular weight SDS-resistant oligomers (Figures 3A and S2). Using $A\beta_{1-42}$ peptides with a tyrosine to alanine or phenylalanine mutation (Aβ42Y10A or Aβ42Y10F) reduced aggregation to the level of untreated $A\beta_{1-42}$ (Figures 3A and S2). In case of the nonmutated $A\beta_{1-42}$, we observed the incorporation of nitrated $A\beta_{1-42}$ into oligomers (Figure 3C). There was a very low amount of nitrated $A\beta_{1-42}$Y10F detectable using the 3NTyr^{10}-Aβ antiserum. Finally, we confirmed our western blot results by detecting an increased formation rate of β sheet amyloid fibril structures of nitrated $A\beta_{1-42}$ using thioflavin T (Figure 3D), which was prevented using the Aβ42Y10F peptide treated with peroxynitrite.

Oxidative conditions can also result in the formation of dityrosine cross-linked proteins (Kato et al., 2000). We therefore investigated whether peroxynitrite is able to induce this modification as well. Using the dityrosine specific antibody IC3 we were able to detect dityrosine cross-linked Aβ in vitro after incubation with increasing concentrations of peroxynitrite (Figure 3E). High concentrations of peroxynitrite resulted in decreased formation of this species, whereas formation of 3NTyr^{10}-Aβ increased even further (Figure 3E). Dityrosine immunoreactivity was also found to be present in the insoluble fractions of aggregated Aβ (Figure 3F). In addition, we performed immunohistochemical analysis of dityrosine with Aβ or 3NTyr^{10}-Aβ in sections of APP/PS1 mice, revealing plaque localization and 3NTyr^{10}-Aβ colocalization of dityrosine

immunoreactivity (Figure 3G). These results suggest that dityrosine formation might also contribute to Aβ aggregation.

NOS2 Deficiency Protects from Behavioral Phenotype and Reduces Aβ Load in APP/PS1 Mice

Looking at effects on spatial memory formation by radial arm maze in 12-month-old APP/PS1 mice, we noticed a strong protection of the NOS2 gene knockout for memory deficits (Figure 4A). In addition, we conducted a therapeutic approach by treating plaque containing mice from 7–12 months with the selective NOS2 inhibitor L-NIL resulting in a reversion of APP/PS1 phenotype concerning reference memory errors (Figure 4A).

Since memory formation and synaptic plasticity are closely connected, we determined the hippocampal long-term potentiation (LTP) of the CA1 region in response to a stimulus of the Schaffer's collaterals in WT, APP/PS1, NOS2 (−/−), APP/PS1 NOS2 (−/−), and APP/PS1 L-NIL treated mice at 4 months (Figure S3). APP/PS1 mice of that age already contain insoluble, high-density amyloid depositions that are positive 3NTyr^{10}-Aβ (Figure S3), that were also found at later age, as well as in AD patients (Figure S3). Analysis of the LTP in APP/PS1 mice showed a reduction LTP, which was not observed in wild-type, NOS2-deficient, or L-NIL-treated mice (Figure S3).

In order to establish a causal link between the observed protective phenotype of NOS2 deficiency and Aβ nitration, we studied the effects of nitrated Aβ on synaptic plasticity. Therefore we treated wild-type (WT) mice acute hippocampal slices with either untreated Aβ$_{1-42}$, nitrated Aβ$_{1-42}$, or a control sample that underwent the same nitration steps without adding Aβ. The application of untreated Aβ$_{1-42}$ decreased LTP 55–60 min after TBS application compared to the slices treated with the control sample ($p = 0.03$, Student's t test); Figure 4B). When Aβ$_{1-42}$ was additionally nitrated, the initial phase of LTP was already significantly decreased compared to controls and this resulted in highly significant differences 55–60 min after TBS ($p = 0.0001$, Student's t test). The average potentiation in control treated slices was 199 ± 8.6% (n = 11 slices /5 animals), Aβ$_{1-42}$ treated slices reached a value of 163% ± 10.9% (n = 11 slices/6 animals), and peroxynitrite treated Aβ$_{1-42}$ led to a potentiation of 141% ± 7.8% (n = 12 slices/7 animals) (Figure 4B). Comparing the results of the nitrated Aβ$_{1-42}$ with the untreated Aβ$_{1-42}$ revealed that the nitrated Aβ$_{1-42}$ showed a significantly reduced potentiation ($t = 60$ min, $p = 0.02$; $t = 80$ min, $p = 0.028$; Student's t test) in comparison to untreated Aβ$_{1-42}$. Overall the strongest effect on synaptic plasticity was observed, when Aβ$_{1-42}$ was nitrated. This is in line with the behavioral data and supports the notion, that nitrated Aβ$_{1-42}$ is more powerful in disturbing processes of synaptic plasticity than Aβ$_{1-42}$ alone.

Subsequent analysis of the mice from the behavioral experiment for Aβ$_{1-40}$ and Aβ$_{1-42}$ revealed a strong reduction in the SDS-soluble fraction (Figures 4C–4F), which was smaller than the reduction of 3NTyr^{10}-Aβ (Figure 2I). Consequently, we observed an increase in the Aβ40/3NTyr^{10}-Aβ and Aβ42/3NTyr^{10}-Aβ ratio (Figure 4G). There were no changes in the expression of APP, neprilysin, and IDE at 12 months of age (Figures 4C and 4D). These findings were confirmed by reduced plaque load in the neocortex and hippocampus in APP/PS1 NOS2 (−/−) mice by thioflavin S staining (Figures 4H and 4I). In keeping with this, loss of NOS2 activity during the phase of plaque formation has a beneficial effect on the formation of Aβ deposits.

Nitrated Aβ Induces Aggregation and Plaque Formation

It is conceivable that the formation of amyloid plaques needs a nucleation event. We therefore tested whether nitrated Aβ$_{1-42}$ can act as a seed of deposition. Testing whether small amounts of nitrated Aβ$_{1-42}$ induces the formation of Aβ oligomers in vitro, we observed a concentration dependent increase in high molecular weight oligomers by western blot analysis (Figure 5A). To test the hypothesis in vivo, we injected 2.5 μl of a 0.5 mg/ml solution of either Aβ$_{1-42}$ or nitrated Aβ$_{1-42}$ aged for 18 hr into the brain of 2.5-month-old APP/PS1 mice. Verification of the injected Aβ peptides by western blot demonstrated the nitration status using the 3NTyr^{10}-Aβ antibody and increased formation of Aβ oligomers using antibody 6E10 (Figure 5B). Analysis of the mice after 8 weeks showed strong 3NTyr^{10}-Aβ immunoreactivity in case of the mice injected with nitrated Aβ$_{1-42}$ (Figure 5D). In addition, nitrated Aβ$_{1-42}$ was able to induce amyloid seeds that were localized distant from the injection side (Figure 5D), that were missing in mice injected with nonnitrated Aβ (Figure 5C). These seeds were composed of nitrated Aβ surrounded by nonnitrated Aβ (Figure 5E), thus resembling the immunomorphological appearance of plaques detected in AD brains. In addition, this species also evoked an increase of Iba1 suggesting a role for microglial activation.

DISCUSSION

Direct propagation of Aβ aggregation by neuroinflammation is unknown; even so, this may be important for the development of disease modifying therapies. In this study, we propose a causative link among the Aβ cascade, activation of NOS2, and the subsequent increase in its reaction product nitric oxide during AD.

NO is a free radical gas that functions physiologically as a diffusible neurotransmitter and signaling molecule. Depending on its concentration it can conduct different actions. At low concentrations, it competes with oxygen for cytochrome oxidase, thereby regulating energy metabolism (Poderoso, 2009). Indirect effects are also mediated by regulating cGMP synthesis and subsequently cGMP-dependent signaling cascades (Poderoso, 2009). However, at high concentration, NOS2-derived NO results in the formation of reactive peroxynitrite, which causes irreversible nitration or nitrosylation of specific amino acid residues, resulting in aberrant protein conformation and function, e.g., in the inhibition of mitochondrial respiration (Szabó et al., 2007).

Previously, nitrosative stress has been demonstrated in disease relevant brain areas in AD (Fernández-Vizarra et al., 2004; Castegna et al., 2003; Colton et al., 2008; Lüth et al., 2002; Hensley et al., 1998). In line with this, induction of NOS2 expression has been demonstrated in AD (Vodovotz et al., 1996; Heneka et al., 2001) and in the Tg2576 AD mouse model (Rodrigo et al., 2004). Since nitric oxide and its reaction products like peroxynitrite are able to introduce posttranslational modifications at cysteine and tyrosine residues (Gow et al., 2004), we

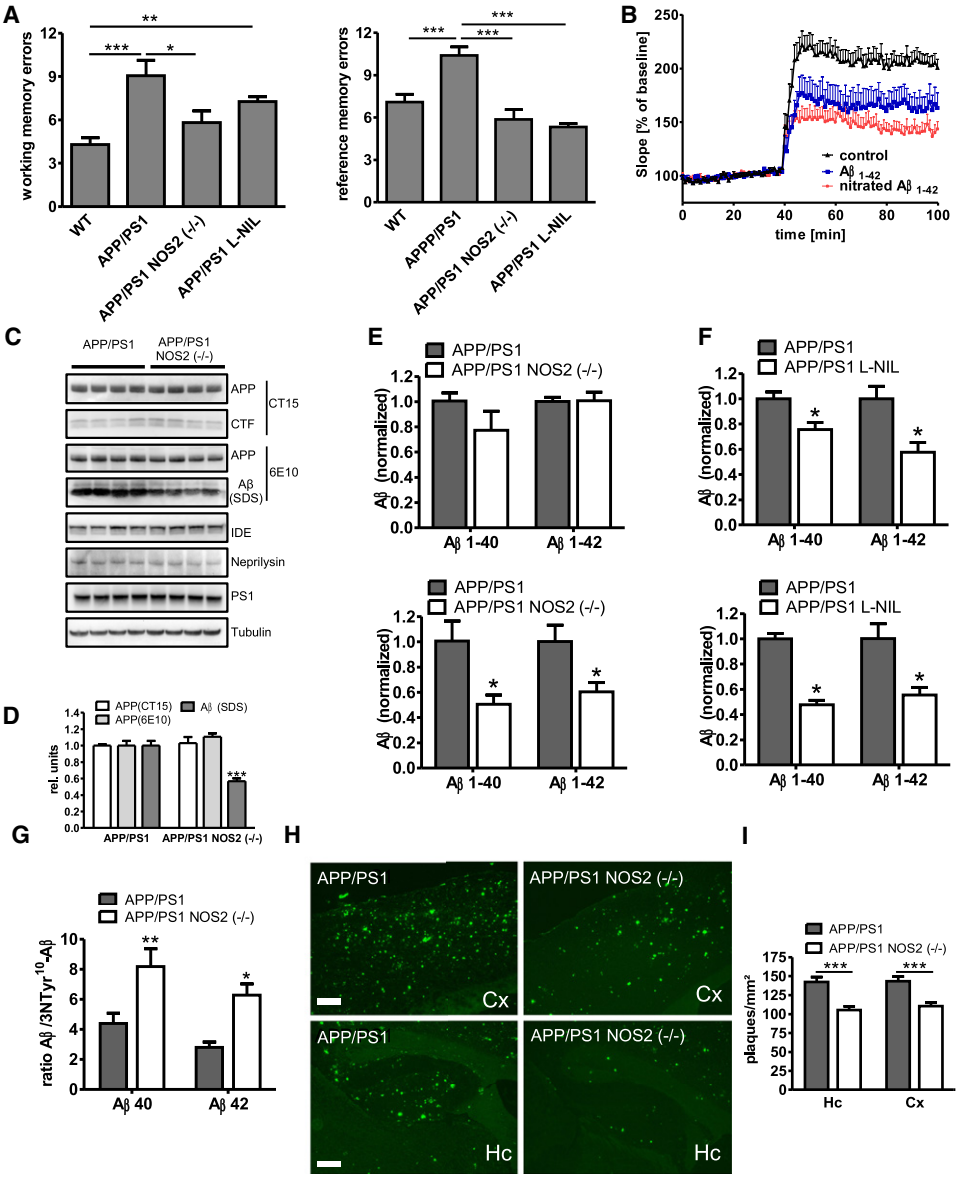

Figure 4. Behavioral Protection and Reduced Aβ Burden in APP/PS1 NOS2 (–/–) Mice

(A) Working memory errors (left panel) and reference memory errors (right panel) of radial arm maze test at 12 months of age (n = 15 ± SEM, ANOVA followed by Student-Newman-Keuls test, *p < 0.05; **p < 0.01; ***p < 0.001).

(B) Acute hippocampal slices from wild-type mice were treated for 40 min with untreated $A\beta_{1-42}$, nitrated $A\beta_{1-42}$, or a control sample that underwent the same nitration steps without adding Aβ (control). LTP induction was measured along the CA3-CA1 Schaffer-collateral pathway (n = 11–12, mean ± SEM); a TBS was applied after 40 min of baseline recording.

(C) Western blot analysis of RIPA and SDS brain extracts of 12-month-old mice.

(D) Quantification of APP expression and SDS-soluble Aβ from C (n = 4 ± SEM, Student's t test, ***p < 0.001).

(E) ELISA quantification of RIPA (upper panel) and SDS (lower panel) fraction for $A\beta_{1-40}$ and 1-42 from 12-month-old APP/PS1 and APP/PS1 NOS2 (−/−) mice (n = 5 ± SEM, Student's t test, *p < 0.05).

(F) 12-month-old APP/PS1- and APP/PS1 L-NIL-treated mice (n = 4 ± SEM, Student's t test, *p < 0.05).

(G) Evaluation of the Aβ and $3NTyr^{10}$-Aβ ELISA data from APP/PS1 and APP/PS1 NOS2 (−/−) mice (n = 4 ± SEM, Students t test, *p < 0.05, **p < 0.01).

(H) Thioflavin S histochemistry of APP/PS1 and APP/PS1 NOS2 (−/−) mice (Hc, hippocampus; Cx, neocortex).

(I) Evaluation of 15 consecutive sections per animal (n = 12 ± SEM, Student's t test, ***p < 0.001).

See also Figure S3.

speculated whether the tyrosine at position 10 of Aβ might be a possible target for NOS2-mediated nitration, thereby influencing its amyloidogenic properties.

Indeed, we were able to demonstrate that Aβ nitrated at tyrosine 10 has an increased propensity to form high molecular weight aggregates in vitro. In line with this, we observed

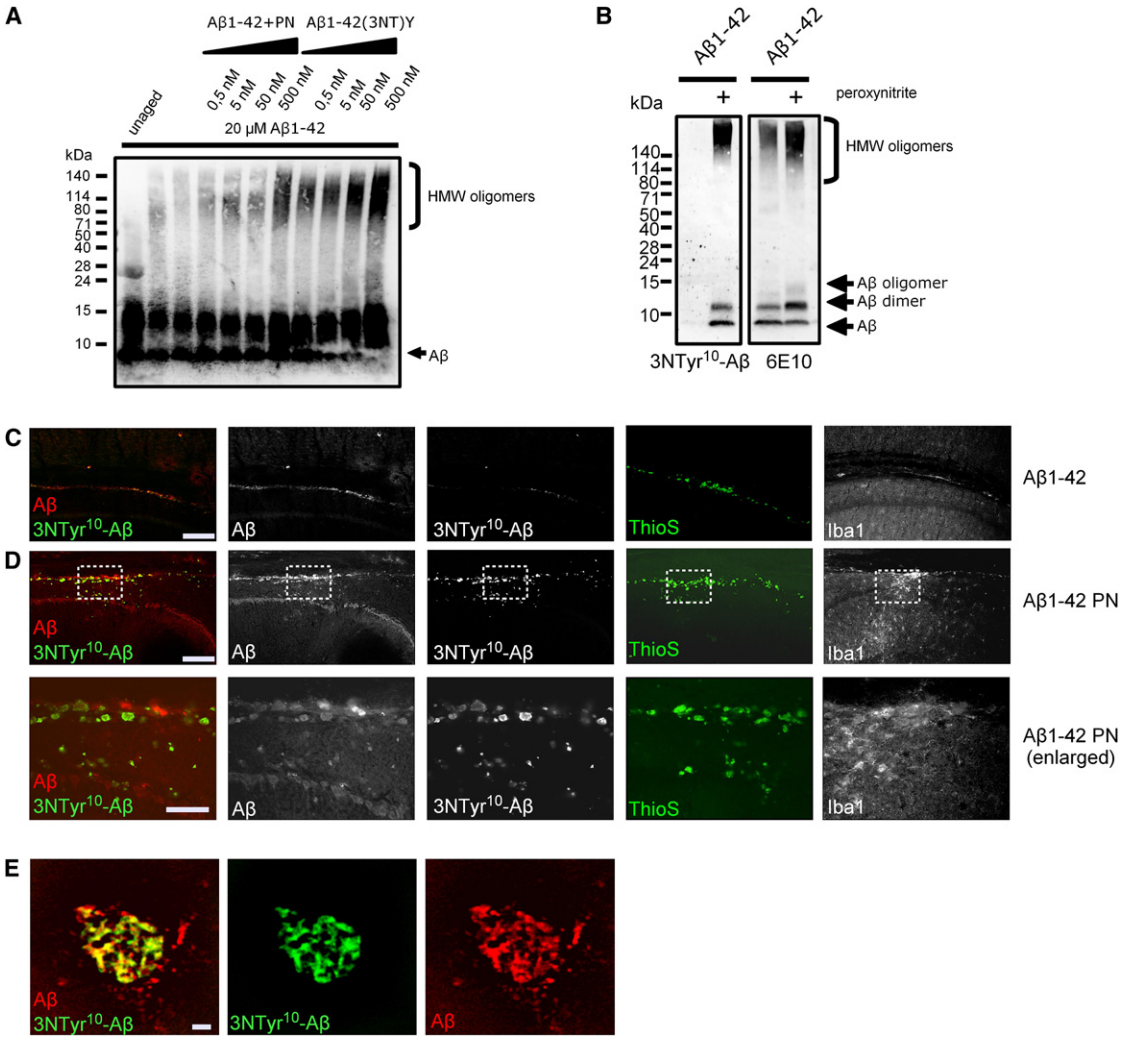

Figure 5. Induction of β-Amyloidosis by 3NTyr^{10}-Aβ

(A) 25 μM Aβ_{1-42} were incubated for 5 hr with increasing amounts of either peroxynitrite (Aβ42PN) treated or synthetically nitrated Aβ_{1-42} (Aβ42(3NT)Y) and oligomeric forms were detected using antibody IC16.

(B) Determination of the nitration and aggregation status of Aβ_{1-42} used for intracerebral injection by western blot using 3NTyr^{10}-Aβ (left panel) and 6E10 (right panel).

(C) Aβ_{1-42} and (D) nitrated Aβ_{1-42} were intracerebrally injected into APP/PS1 mice. Sections were analyzed 8 weeks later using antibodies IC16, 3NTyr^{10}-Aβ and Iba1, and by thioflavin S histochemistry. Bar = 200 μM, lower panel bar = 50 μm.

(E) Enlargement of a newly seeded plaque-like structure from (B). Bar = 2 μM.

a protective effect on amyloid plaque formation and memory function by deleting the NOS2 gene from APP/PS1 mice. Our data are in accordance with a previous report using the Tg2576 mouse model crossbred with the human PS1 A246E mutation (Nathan et al., 2005). In addition, we observed similar effects after oral long-term application of the NOS2-specific substrate analog inhibitor L-NIL. Besides its selectivity (23-fold over NOS1 and 49-fold over NOS3) (Moore et al., 1994; Alderton et al., 2001), the oral bioavailability and its brain penetration have been demonstrated (Rebello et al., 2002). Of note, the safety of L-NIL has already been demonstrated in patients suffering from asthma and in healthy controls (Hansel et al., 2003).

Importantly, improved spatial learning and memory in NOS2 (−/−) or L-NIL-treated APP/PS1 mice may well be causally linked to the nitration of Aβ_{1-42} as the latter decreased hippocampal long-term potentiation more effectively when compared to nonnitrated Aβ_{1-42}, suggesting that nitration of Aβ may exert a direct effect on synaptic transmission even before its deposition in plaques. This is additionally supported by the observation that deletion of NOS2 or L-NIL treatment in young APP/PS1 mice results in improved LTP. Nevertheless, additional NO-mediated effects, likely to be independent of nitrated Aβ, that protect from Aβ-induced suppression of LTP have been reported (Wang et al., 2004). Further, the reduction of Aβ in APP/PS1

NOS2 (−/−) mice may lower the production of proinflammatory cytokines by activated microglia and astrocytes and thereby protect from LTP suppression (Hauss-Wegrzyniak et al., 2002; Griffin et al., 2006; Tancredi et al., 1992, 2000).

In contrast, a beneficial role of NOS2 in an AD mouse model expressing the APP Swedish mutation has been suggested. Deletion of NOS2 resulted in increased Aβ deposition and improved spatial memory (Wilcock et al., 2008; Colton et al., 2006, 2008). Even so there has been no mechanistic explanation for the changes in Aβ burden in this study, a main difference to our study is the usage of an AD mouse model lacking a PS1 transgene, which may account for the opposite effects observed in this study and in a previous one (Nathan et al., 2005). Colton et al. argued that the enhanced upregulation of NOS2 is an overexpression artifact of the PS1 transgene caused by an inflammatory response within resident immune cells, as evidenced in vitro by Lee et al. (2002). However, such an effect has not been observed in rodent AD models or in patients with sporadic AD. Nevertheless, an impact of the PS1 ΔExon 9 transgene on immune cells, like microglia cells, is unlikely, since the prion promoter driven APP/PS1 mouse model system used in this study results in the expression of both transgenes (APPsw and PS1 ΔExon 9) almost exclusively confined to neurons (Kretzschmar et al., 1986).

Based on the evidence presented in this study, we propose that the observed decrease in amyloid burden in NOS2 knockout or L-NIL-treated APP/PS1 mice is attributed to a new NO-induced posttranslational Aβ modification that critically increases its aggregation and solubility profile. This is supported by the observation that nitrated Aβ is localized to SDS-soluble fractions in APP/PS1 mice. In addition, nitrated Aβ was not detectable in the CSF nor in RIPA-soluble tissue fraction but in SDS-soluble fractions of AD brains. In keeping with this, nitrated Aβ was immunohistochemically localized to the core of plaques of APP/PS1 mice and human AD brains, suggesting that it serves as a seeding structure. In addition, immunohistometrical plaque analysis of APP/PS1 mice at 5 and 9 months of age revealed that the $3NTyr^{10}$-Aβ positive cores of amyloid plaques do not grow over this period of time, whereas total plaque size increased. This suggests that nitration of Aβ defines the number of amyloid plaques, but not their size once formed.

Supporting this assumption, injection of nitrated Aβ resulted in seeding of microplaques within a short period of time. Hence, this posttranslational Aβ modification may explain why injection of synthetic Aβ into AD mouse models fails as a seeding agent in AD mouse models (Meyer-Luehmann et al., 2006; Eisele et al., 2009), in contrast to the use of brain homogenates from murine AD models or human AD brains, both of which supposedly contain nitrated Aβ. Nevertheless, we neither can rule out other NO-induced mechanisms including synaptic failure and neuronal cell death (Nakamura and Lipton, 2009) contributing to the protective effect of NOS2 deletion.

The observation that expression of murine APP, lacking the tyrosine within the Aβ domain, does not result in Aβ deposition in mice (Jankowsky et al., 2007) but in rodents endogenously possessing this tyrosine (Inestrosa et al., 2005), suggests a critical role for this amino acid in β-amyloidosis. Nevertheless, this has to be confirmed experimentally.

It has been known that fibrillar Aβ is able to activate microglia (Meda et al., 1995), resulting in the induction of NOS2 expression (Combs et al., 2001; Tran et al., 2001; Ishii et al., 2000). This in turn may generate a self-perpetuating cycle of Aβ aggregation and NO production that contributes to the chronicity and progression of AD.

One might argue that the nitration yields under inflammatory conditions are relatively low, resulting in the modification of only 0.01%–0.05% of all tyrosine residues (Radi, 2004). However, in a gain-of-function scenario, nitrated Aβ may focally accumulate over a life time, thereby facilitating the rate-limiting nucleation step for the initiation of plaque deposition. In support of this, an 8-fold increase of nitrated proteins has been observed in AD (Smith et al., 1997). Further, assessing the overall amount of nitrated proteins in the hippocampus of MCI patients, an equivalent to the nitration of purified BSA achieved with 27 mM peroxynitrite was estimated (Butterfield et al., 2007), exposing the drastic consequences from chronic exposure to nitric oxide radicals.

Nitration induced oligomerization has also been reported for other disease-related proteins. Recently, the effects of peroxynitrite on oligomerization of α-synuclein by formation of covalent dityrosine cross-links has been demonstrated (Souza et al., 2000). In addition, a widespread accumulation of nitrated α-synuclein has found in several neurodegenerative diseases associated with Lewy bodies (Giasson et al., 2000). Furthermore, the presence of nitrated tau in AD brains and its peroxynitrite-induced oligomerization has been observed (Horiguchi et al., 2003).

Together, our data identify a posttranslational modification of Aβ and characterize its functional implication that provides evidence for a link between the amyloid and neuroinflammatory component of AD. We think that $3NTyr^{10}$-Aβ may be a promising target for a course modifying therapy of AD. The application of specific inhibitors of NOS2 may therefore open a new therapeutic avenue in AD.

EXPERIMENTAL PROCEDURES

Animals

APP/PS1 transgenic animals (#005864, The Jackson Laboratory) (Jankowsky et al., 2001) and NOS2-deficient animals (# 002609, The Jackson Laboratory) (Laubach et al., 1995) were both of the BC57/Bl6 genetic background. L-NIL was given orally in the water either from 2–3-months or 7–12 months of age (8 mg/kg body weight). L-NIL was replaced daily. Mice were housed under standard conditions at 22°C and a 12 hr light-dark cycle with free access to food and water. Animal care and handling was performed according to the declaration of Helsinki and approved by the local ethical committees.

Radial Arm Maze

Learning and memory testing was conducted in an eight arm maze as previously described (Olton, 1987). Briefly, each arm of the maze was 60 cm long and 6 cm wide and extended from an octagonal central platform 10 cm in diameter. One centimeter deep food cups were placed 2 cm from the end of each arm. Several visual cues were put outside of the maze, and the room was lit dimly. Mice were trained for 3 days. During each training session, the mouse was placed on the center platform and allowed to move freely in the maze to obtain food pellets, which were presented in all eight arms, for 10 min. Starting day 4, the mice were tested once per day for a total of 14 days. During the test sessions, four randomly selected arms were baited

with one pellet of food each; the baited arms were kept unchanged throughout the experiment. The mouse was allowed to move until it collected the four pellets or until 10 min passed, whichever occurred first. Parameters evaluated were reentry into baited arms that had been visited during the session (working memory error) and entries into unbaited arms (reference memory error).The task was considered learned when the working memory error was zero and the average reference memory error was one or less than one in three successive sessions.

Brain Protein Extraction

Snap-frozen brain hemispheres were extracted as previously described (Jardanhazi-Kurutz et al., 2010).

Tissue Preparation

After completion of the behavioral testing, mice were anesthetized using isoflurane and transcardially perfused with 15 ml phosphate-buffered saline. The brains were removed from the skull. One hemisphere was frozen immediately for biochemical analysis and the other was frozen in a mixture of dry ice and isopentane for histology.

Protein Blotting

Samples were separated by 4%–12% NuPAGE (Invitrogen) using MES or MOPS buffer and transferred to nitrocellulose membranes. APP and Aβ were detected using antibody 6E10 (Covance) and the C-terminal APP antibody 140 (CT15) (Wahle et al., 2006), IDE using antibody PC730 (Calbiochem), neprilysin using antibody 56C6 (Santa Cruz), presenilin using antibody PS1-NT (Calbiochem), and tubulin using antibody E7 (Developmental Studies Hybridoma Bank). For dot blot analysis, 10 μl samples containing 25 μM peptide were mixed with 200 μl PBS and transferred to nitrocellulose membranes. Immunoreactivity was detected by enhanced chemiluminescence reaction (Millipore; luminescence intensities were analyzed using Chemidoc XRS documentation system [Bio-Rad]).

ELISA

Quantitative determination of Aβ was performed using the human amyloid $A\beta_{1-40}$ and $A\beta_{1-42}$ ELISA kits (The Genetics Company) according to the manufacturer's protocol. Human samples were analyzed using an electrochemoluminescence ELISA for $A\beta_{1-38}$, $A\beta_{1-40}$, and $A\beta_{1-42}$ (Mesoscale). pTau181 was determined using the INNOTEST PHOSPHO-TAU(181P) ELISA (Innogenetics). For $3NTyr^{10}$-Aβ, 96-well plates were coated with 50 μl 20 μg/ml $3NTyr^{10}$-Aβ antiserum in PBS 4 hr at 20°C. Plates were blocked with 3% BSA in TBS. Ten microliters of 2% SDS fractions from mouse brain were diluted with 50 μl 2% Tx-100, 25 mM Tris-HCl (pH 7.5), and 150 mM NaCl. Fifty microliters samples were incubated for 18 hr at 4°C, washed with TBST, and incubated with 6E10 diluted 1:10,000 in TBST for 2 hr. Wells were washed, and 50 μl HRP-goat anti-mouse antibody diluted 1:10,000 with TBST was added for 2 hr. After washing, 50 μl TMB ultra substrate (Thermo) was added and the reaction was stopped using 2M sulfuric acid. Absorption was determined at 450 nm using an infinite 200 plate reader (Tecan).

Histology

Serial sagittal cryosections (20 μm) were fixed in 4% paraformaldehyde, and immunostaining was performed using antiserum $3NTyr^{10}$-Aβ (1:200), antibody IC16 (Jäger et al., 2009) against human Aβ1-15 (1:400), rabbit polyclonal antiserum 2964 against fibrillar $A\beta_{1-42}$ (Wahle et al., 2006), and antibody IC3 (Kato et al., 2000) against dityrosine (1:100). Thioflavin S staining was performed on paraformaldehyde-fixed cryosections. Slices were rinsed in water, incubated in 0.01% thioflavin S in 50% ethanol, and differentiated in 50% ethanol. Sections were analyzed using a BX61 microscope equipped with a disk scanning unit to achieve confocality (Olympus). Image stacks were deconvoluted using Cell^P (Olympus). Quantitative assessment of plaque areas was done using ImageJ (NIH; Bethesda, MD) software.

Immunoprecipitation

Brains were extracted as described before with the following changes: homogenates were centrifuged at 100,000 × g for 20 min to generate the PBS fraction. The pellet of the SDS fraction was extracted with 1,1,1-6,6,6-hexafluoroisopropanol (HFIP), dried in a speed vac and resuspended in 2% SDS. For immunoprecipitation, samples were diluted in 5 vol. of RIPA buffer and incubated for 18 hr at 4°C with protein G agarose and 3 μl $3\text{-}NTyr^{10}$-Aβ. Precipitates were washed twice with RIPA and once with PBS and immunoblotted using antibody 6E10.

Aβ Aggregation Assay

$A\beta_{1-42}$, $A\beta_{1-42}$ Y10F (Peptide Specialty Laboratories) were solubilized as previously described (Teplow, 2006). For nitration, samples were incubated with 0.25–0.5 mM peroxynitrite in water while vortexing. Aggregation was started by diluting samples to 25 μM using 50 mM Tris-HCl (pH 7). Samples were separated by 4%–12% NuPAGE, and aggregates were detected using antibody 6E10 (Signet) and $3\text{-}NTyr^{10}$-Aβ. Aggregation was expressed as a ratio between the signal above 30 kDa and the Aβ monomer, normalized to the 0 time point of $A\beta_{1-42}$. Thioflavin T fluorescence assays were performed as described previously (LeVine, 1999). Fluorescence was read at 446 nm (excitation) and 482 nm (emission) using a fluorescence spectrophotometer (Varian). For determination of the solubility of dityrosine linked Aβ, samples were aged for 5 hr and centrifuged at 10, 000 × g for 1 hr. Pellets were resuspended in 50 mM Tris (pH 7) and analyzed by dot blot.

3′-Nitrotyrosine-Specific Amyloid β Antiserum

The antiserum recognizing the $3\text{-}NTyr^{10}$-Aβ was generated by rabbit immunization using the synthetically nitrated peptide FRHDSG(3NT-Y)EVHHQ (Eurogentech). The resulting serum was first immunopurified against the nitrated peptide and subsequently antibodies against the unmodified peptide were removed by immunochromatography against the peptide FRHDSGYEVHHQ.

Human Samples

Human brain samples were from the parietal cortex of 5 age control and 8 diagnosed AD patients (Braak staging V–VI, CERAD B–C). The post mortem interval (PMI) was comparable among groups ranging from 4–48 hr. Samples were extracted as the mouse brains described above with the exception that instead of RIPA buffer 25 mM Tris-HCl (pH 7.5), 150 mM NaCl, 1% Tx-100 was used. CSF samples were from 10 control, 10 mild cognitive impaired, and 10 diagnosed AD patients.

Intracerebral Injections

Two and one-half-month-old APP/PS1 mice (n = 3) were anesthetized with ketamine (30 mg/kg) and xylazine (4 mg/kg). Two and one-half microliters of 0.25 mg/ml Aβ solutions were injected intracortically into the right hemisphere anteroposterior –2.5, lateral 2.0 at 1.0 mm (cortex), and in addition at 1.5 mm (hippocampus) depth relative to the bregma at a rate of 1 μl/min. Control solutions were injected into the left hemisphere, accordingly. Mice were sacrificed 8 weeks later. Cryosections in the proximity of the injection channel were stained using antibodies IC16, 3NTyr10-Aβ, and anti-Iba1 (1:400, Wako).

Slice Preparation

Acute hippocampal transversal slices were prepared from 40- to 60-day-old wild-type C57BL/6 mice (P40–60) according to standard procedures. In brief, mice were anesthetized and decapitated, the brain was quickly transferred into ice-cold carbogenated (95% O_2, 5% CO_2) artificial cerebrospinal fluid (ACSF) which contained 125.0 mM NaCl, 2.0 mM KCl, 1.25 mM NaH2PO4, 2.0 mM MgCl2, 26.0 mM NaHCO3, 2.0 mM CaCl2, 25.0 mM glucose. Hippocampi were dissected and cut into 400 μm thick transversal slices with a vibratome (Leica, VT1200S). Slices were maintained in carbogenated ACSF at room temperature for at least 1.5 hr before recording. Recordings were performed in a submerged recording chamber at 32°C.

Electrophysiology

To study the effect of acute Aβ application on LTP three different samples were used: (1) untreated $A\beta_{1-42}$, (2) nitrated $A\beta_{1-42}$ with peroxynitrite (500 μM), (3) a control sample where all nitration steps were performed without adding $A\beta_{1-42}$ (control). $A\beta_{1-42}$ was prepared as previously described (Teplow, 2006). Nitration was carried out by adding water diluted peroxynitrite to $A\beta_{1-42}$ or control sample solution while vortexing. The solutions were freshly

prepared in carbonated ACSF from frozen aliquots with a final concentration of 500 nM. Silicon tubing was used and BSA (0.1 mg/ml) was added to the peptide containing as well as to the control solutions (Chen et al., 1999). Tubings and beakers were washed with ACSF containing BSA to prevent sticking of the peptide. A closed-loop perfusion system with a total volume of 30 ml perfusion medium was used. The perfusion rate in the recording chamber was constantly kept at 1.0 ml/min. After placing the slices in the submerged recording chamber field excitatory postsynaptic potentials (fEPSPs) were recorded in stratum radiatum of CA1 region with a borosilicate glass micropipette (resistance 3–15 MΩ) filled with 3 M NaCl at a depth of 90–120 μm. Monopolar tungsten electrodes were used for stimulating the Schaffer collaterals at a frequency of 0.1 Hz. Stimulation was set to elicit a fEPSP with a slope of 40% of maximum for LTP recordings and 60% for LTD recordings. After 20 min prebaseline stimulation, the three different samples were washed into the chamber and the baseline was recorded for another 40 min. LTP was induced by applying theta-burst stimulation (TBS). One burst consists of four pulses at 100 Hz, repeated 10 times in an 200 ms interval. Three such bursts were used to induce LTP at 0.1 Hz.

To study the effect of NOS2 deficiency on LTP, brains were dissected and sagittally sliced in 400 μm sections using a vibratome (Camden Instruments, Integraslice 7550 PSDS). The recording of the field excitatory postsynaptic potential (fEPSP) was initiated after 15 min of basal recording. Basal synaptic transmission (BST) was assessed by plotting the current (mA) against the peak amplitudes of fEPSP to generate input-output relations. Paired-pulse facilitation (PPF) were recorded by applying interstimulus intervals of 30, 50, 75, and 100 ms. For long-term potentiation (LTP) experiments a 15 min baseline were recorded with a interpulse interval of 1 min at an intensity that evoked a response approximately 30% of maximum fEPSP. The LTP was induced by a theta burst consisting of 4 trains of 10 pulses at 100 Hz separated by 200 ms.

Data Analysis

Data were collected, stored and analyzed with LABVIEW software (National Instruments, Austin, TX). The initial slope of fEPSPs elicited by stimulation of the Schaffer collaterals was measured over time, normalized to baseline, which was the mean response of the 40 min before TBS application and plotted as average ± SEM. Parameters leading to an exclusion of single experiments were (1) an unstable baseline (variability more than ± 10%) or (2) a large population spike after TBS application producing an artificially large LTP.

SUPPLEMENTAL INFORMATION

Supplemental Information includes three figures and Supplemental Experimental Procedures and can be found with this article online at doi:10.1016/j.neuron.2011.07.001.

ACKNOWLEDGMENTS

We thank Drs. Mathias Jucker and Gary Landreth for critically reading the manuscript. We are grateful to Drs. Sascha Weggen and Claus Pietrzik for providing antibody IC16, Dr. Yoji Kato for providing antibody IC3, and to Claudia Hülsmann, Daisy Axt, Ana Viera-Saecker, and Anna-Maria Mehlich for excellent technical assistance. The E7 antibody developed by M. Klymkowsky was obtained from the Developmental Studies Hybridoma Bank. This study was supported by the Deutsche Forschungsgemeinschaft (HE 3350/4-1 und HE 3350 4-2; KFO177, TP4) to M.T.H. M.P.K. and M.T.H. conceived the experiments. M.P.K., M.H., M.T.H., A.D., T.H., S. Kumar, and S. König carried out experiments. M.P.K., M.H., A.D., S. Kumar, S. König, M.K., and M.T.H. designed and carried out data analysis. S.R. and F.J. provided and characterized human samples. M.P.K., S. Kumar, S. König, D.T., J.W., T.K., M.K., and M.T.H. cowrote the paper. All authors participated in the discussion.

Accepted: July 1, 2011
Published: September 7, 2011

REFERENCES

Alderton, W.K., Cooper, C.E., and Knowles, R.G. (2001). Nitric oxide synthases: structure, function and inhibition. Biochem. J. *357*, 593–615.

Beal, M.F. (2000). Energetics in the pathogenesis of neurodegenerative diseases. Trends Neurosci. *23*, 298–304.

Butterfield, D.A., Reed, T.T., Perluigi, M., De Marco, C., Coccia, R., Keller, J.N., Markesbery, W.R., and Sultana, R. (2007). Elevated levels of 3-nitrotyrosine in brain from subjects with amnestic mild cognitive impairment: implications for the role of nitration in the progression of Alzheimer's disease. Brain Res. *1148*, 243–248.

Castegna, A., Thongboonkerd, V., Klein, J.B., Lynn, B., Markesbery, W.R., and Butterfield, D.A. (2003). Proteomic identification of nitrated proteins in Alzheimer's disease brain. J. Neurochem. *85*, 1394–1401.

Chen, G., Kolbeck, R., Barde, Y.A., Bonhoeffer, T., and Kossel, A. (1999). Relative contribution of endogenous neurotrophins in hippocampal long-term potentiation. J. Neurosci. *19*, 7983–7990.

Colton, C.A., Vitek, M.P., Wink, D.A., Xu, Q., Cantillana, V., Previti, M.L., Van Nostrand, W.E., Weinberg, J.B., Dawson, H., and Dawson, H. (2006). NO synthase 2 (NOS2) deletion promotes multiple pathologies in a mouse model of Alzheimer's disease. Proc. Natl. Acad. Sci. USA *103*, 12867–12872.

Colton, C.A., Wilcock, D.M., Wink, D.A., Davis, J., Van Nostrand, W.E., and Vitek, M.P. (2008). The effects of NOS2 gene deletion on mice expressing mutated human AbetaPP. J. Alzheimers Dis. *15*, 571–587.

Combs, C.K., Karlo, J.C., Kao, S.C., and Landreth, G.E. (2001). beta-Amyloid stimulation of microglia and monocytes results in TNFalpha-dependent expression of inducible nitric oxide synthase and neuronal apoptosis. J. Neurosci. *21*, 1179–1188.

Eisele, Y.S., Bolmont, T., Heikenwalder, M., Langer, F., Jacobson, L.H., Yan, Z.-X., Roth, K., Aguzzi, A., Staufenbiel, M., Walker, L.C., and Jucker, M. (2009). Induction of cerebral beta-amyloidosis: intracerebral versus systemic Abeta inoculation. Proc. Natl. Acad. Sci. USA *106*, 12926–12931.

Ferger, B., Themann, C., Rose, S., Halliwell, B., and Jenner, P. (2001). 6-hydroxydopamine increases the hydroxylation and nitration of phenylalanine in vivo: implication of peroxynitrite formation. J. Neurochem. *78*, 509–514.

Fernández-Vizarra, P., Fernández, A.P., Castro-Blanco, S., Encinas, J.M., Serrano, J., Bentura, M.L., Muñoz, P., Martínez-Murillo, R., and Rodrigo, J. (2004). Expression of nitric oxide system in clinically evaluated cases of Alzheimer's disease. Neurobiol. Dis. *15*, 287–305.

Giasson, B.I., Duda, J.E., Murray, I.V., Chen, Q., Souza, J.M., Hurtig, H.I., Ischiropoulos, H., Trojanowski, J.Q., and Lee, V.M. (2000). Oxidative damage linked to neurodegeneration by selective alpha-synuclein nitration in synucleinopathy lesions. Science *290*, 985–989.

Glass, C.K., Saijo, K., Winner, B., Marchetto, M.C., and Gage, F.H. (2010). Mechanisms underlying inflammation in neurodegeneration. Cell *140*, 918–934.

Gow, A.J., Farkouh, C.R., Munson, D.A., Posencheg, M.A., and Ischiropoulos, H. (2004). Biological significance of nitric oxide-mediated protein modifications. Am. J. Physiol. Lung Cell. Mol. Physiol. *287*, L262–L268.

Griffin, R., Nally, R., Nolan, Y., McCartney, Y., Linden, J., and Lynch, M.A. (2006). The age-related attenuation in long-term potentiation is associated with microglial activation. J. Neurochem. *99*, 1263–1272.

Hansel, T.T., Kharitonov, S.A., Donnelly, L.E., Erin, E.M., Currie, M.G., Moore, W.M., Manning, P.T., Recker, D.P., and Barnes, P.J. (2003). A selective inhibitor of inducible nitric oxide synthase inhibits exhaled breath nitric oxide in healthy volunteers and asthmatics. FASEB J. *17*, 1298–1300.

Hauss-Wegrzyniak, B., Lynch, M.A., Vraniak, P.D., and Wenk, G.L. (2002). Chronic brain inflammation results in cell loss in the entorhinal cortex and impaired LTP in perforant path-granule cell synapses. Exp. Neurol. *176*, 336–341.

He, W., and Barrow, C.J. (1999). The A beta 3-pyroglutamyl and 11-pyroglutamyl peptides found in senile plaque have greater beta-sheet forming and

aggregation propensities in vitro than full-length A beta. Biochemistry *38*, 10871–10877.

Heneka, M.T., Wiesinger, H., Dumitrescu-Ozimek, L., Riederer, P., Feinstein, D.L., and Klockgether, T. (2001). Neuronal and glial coexpression of argininosuccinate synthetase and inducible nitric oxide synthase in Alzheimer disease. J. Neuropathol. Exp. Neurol. *60*, 906–916.

Hensley, K., Maidt, M.L., Yu, Z., Sang, H., Markesbery, W.R., and Floyd, R.A. (1998). Electrochemical analysis of protein nitrotyrosine and dityrosine in the Alzheimer brain indicates region-specific accumulation. J. Neurosci. *18*, 8126–8132.

Horiguchi, T., Uryu, K., Giasson, B.I., Ischiropoulos, H., LightFoot, R., Bellmann, C., Richter-Landsberg, C., Lee, V.M., and Trojanowski, J.Q. (2003). Nitration of tau protein is linked to neurodegeneration in tauopathies. Am. J. Pathol. *163*, 1021–1031.

Inestrosa, N.C., Reyes, A.E., Chacón, M.A., Cerpa, W., Villalón, A., Montiel, J., Merabachvili, G., Aldunate, R., Bozinovic, F., and Aboitiz, F. (2005). Human-like rodent amyloid-beta-peptide determines Alzheimer pathology in aged wild-type Octodon degu. Neurobiol. Aging *26*, 1023–1028.

Ishii, K., Muelhauser, F., Liebl, U., Picard, M., Kühl, S., Penke, B., Bayer, T., Wiessler, M., Hennerici, M., Beyreuther, K., et al. (2000). Subacute NO generation induced by Alzheimer's beta-amyloid in the living brain: reversal by inhibition of the inducible NO synthase. FASEB J. *14*, 1485–1489.

Jäger, S., Leuchtenberger, S., Martin, A., Czirr, E., Wesselowski, J., Dieckmann, M., Waldron, E., Korth, C., Koo, E.H., Heneka, M., et al. (2009). alpha-secretase mediated conversion of the amyloid precursor protein derived membrane stub C99 to C83 limits Abeta generation. J. Neurochem. *111*, 1369–1382.

Jankowsky, J.L., Slunt, H.H., Ratovitski, T., Jenkins, N.A., Copeland, N.G., and Borchelt, D.R. (2001). Co-expression of multiple transgenes in mouse CNS: a comparison of strategies. Biomol. Eng. *17*, 157–165.

Jankowsky, J.L., Younkin, L.H., Gonzales, V., Fadale, D.J., Slunt, H.H., Lester, H.A., Younkin, S.G., and Borchelt, D.R. (2007). Rodent A beta modulates the solubility and distribution of amyloid deposits in transgenic mice. J. Biol. Chem. *282*, 22707–22720.

Jardanhazi-Kurutz, D., Kummer, M.P., Terwel, D., Vogel, K., Dyrks, T., Thiele, A., and Heneka, M.T. (2010). Induced LC degeneration in APP/PS1 transgenic mice accelerates early cerebral amyloidosis and cognitive deficits. Neurochem. Int. *57*, 375–382.

Kato, Y., Wu, X., Naito, M., Nomura, H., Kitamoto, N., and Osawa, T. (2000). Immunochemical detection of protein dityrosine in atherosclerotic lesion of apo-E-deficient mice using a novel monoclonal antibody. Biochem. Biophys. Res. Commun. *275*, 11–15.

Kretzschmar, H.A., Prusiner, S.B., Stowring, L.E., and DeArmond, S.J. (1986). Scrapie prion proteins are synthesized in neurons. Am. J. Pathol. *122*, 1–5.

Laubach, V.E., Shesely, E.G., Smithies, O., and Sherman, P.A. (1995). Mice lacking inducible nitric oxide synthase are not resistant to lipopolysaccharide-induced death. Proc. Natl. Acad. Sci. USA *92*, 10688–10692.

Lee, J., Chan, S.L., and Mattson, M.P. (2002). Adverse effect of a presenilin-1 mutation in microglia results in enhanced nitric oxide and inflammatory cytokine responses to immune challenge in the brain. Neuromolecular Med. *2*, 29–45.

LeVine, H., 3rd. (1999). Quantification of beta-sheet amyloid fibril structures with thioflavin T. Methods Enzymol. *309*, 274–284.

Lüth, H.-J., Münch, G., and Arendt, T. (2002). Aberrant expression of NOS isoforms in Alzheimer's disease is structurally related to nitrotyrosine formation. Brain Res. *953*, 135–143.

Meda, L., Cassatella, M.A., Szendrei, G.I., Otvos, L., Jr., Baron, P., Villalba, M., Ferrari, D., and Rossi, F. (1995). Activation of microglial cells by beta-amyloid protein and interferon-gamma. Nature *374*, 647–650.

Meyer-Luehmann, M., Coomaraswamy, J., Bolmont, T., Kaeser, S., Schaefer, C., Kilger, E., Neuenschwander, A., Abramowski, D., Frey, P., Jaton, A.L., et al. (2006). Exogenous induction of cerebral beta-amyloidogenesis is governed by agent and host. Science *313*, 1781–1784.

Moore, W.M., Webber, R.K., Jerome, G.M., Tjoeng, F.S., Misko, T.P., and Currie, M.G. (1994). L-N6-(1-iminoethyl)lysine: a selective inhibitor of inducible nitric oxide synthase. J. Med. Chem. *37*, 3886–3888.

Nakamura, T., and Lipton, S.A. (2009). Cell death: protein misfolding and neurodegenerative diseases. Apoptosis *14*, 455–468.

Nathan, C., Calingasan, N., Nezezon, J., Ding, A., Lucia, M.S., La Perle, K., Fuortes, M., Lin, M., Ehrt, S., Kwon, N.S., et al. (2005). Protection from Alzheimer's-like disease in the mouse by genetic ablation of inducible nitric oxide synthase. J. Exp. Med. *202*, 1163–1169.

Olton, D.S. (1987). The radial arm maze as a tool in behavioral pharmacology. Physiol. Behav. *40*, 793–797.

Petersson, A.S., Steen, H., Kalume, D.E., Caidahl, K., and Roepstorff, P. (2001). Investigation of tyrosine nitration in proteins by mass spectrometry. J. Mass Spectrom. *36*, 616–625.

Poderoso, J.J. (2009). The formation of peroxynitrite in the applied physiology of mitochondrial nitric oxide. Arch. Biochem. Biophys. *484*, 214–220.

Querfurth, H.W., and LaFerla, F.M. (2010). Alzheimer's disease. N. Engl. J. Med. *362*, 329–344.

Radi, R. (2004). Nitric oxide, oxidants, and protein tyrosine nitration. Proc. Natl. Acad. Sci. USA *101*, 4003–4008.

Rebello, S., Zhu, B., McMonagle-Strucko, K., and Pulicicchio, J. (2002). Pharmacokinetic and pharmacodynamic evaluation of inhibitors of inducible NitricOxide Synthase (iNOS) in mice. AAPS PharmSci. *4* (*Suppl 1*). http://www.aapsj.org/abstracts/AM_2002/AAPS2002-002237.pdf.

Rodrigo, J., Fernández-Vizarra, P., Castro-Blanco, S., Bentura, M.L., Nieto, M., Gómez-Isla, T., Martínez-Murillo, R., MartInez, A., Serrano, J., and Fernández, A.P. (2004). Nitric oxide in the cerebral cortex of amyloid-precursor protein (SW) Tg2576 transgenic mice. Neuroscience *128*, 73–89.

Shivers, B.D., Hilbich, C., Multhaup, G., Salbaum, M., Beyreuther, K., and Seeburg, P.H. (1988). Alzheimer's disease amyloidogenic glycoprotein: expression pattern in rat brain suggests a role in cell contact. EMBO J. *7*, 1365–1370.

Smith, M.A., Richey Harris, P.L., Sayre, L.M., Beckman, J.S., and Perry, G. (1997). Widespread peroxynitrite-mediated damage in Alzheimer's disease. J. Neurosci. *17*, 2653–2657.

Souza, J.M., Giasson, B.I., Chen, Q., Lee, V.M., and Ischiropoulos, H. (2000). Dityrosine cross-linking promotes formation of stable alpha -synuclein polymers. Implication of nitrative and oxidative stress in the pathogenesis of neurodegenerative synucleinopathies. J. Biol. Chem. *275*, 18344–18349.

Szabó, C., Ischiropoulos, H., and Radi, R. (2007). Peroxynitrite: biochemistry, pathophysiology and development of therapeutics. Nat. Rev. Drug Discov. *6*, 662–680.

Tancredi, V., D'Arcangelo, G., Grassi, F., Tarroni, P., Palmieri, G., Santoni, A., and Eusebi, F. (1992). Tumor necrosis factor alters synaptic transmission in rat hippocampal slices. Neurosci. Lett. *146*, 176–178.

Tancredi, V., D'Antuono, M., Cafè, C., Giovedì, S., Buè, M.C., D'Arcangelo, G., Onofri, F., and Benfenati, F. (2000). The inhibitory effects of interleukin-6 on synaptic plasticity in the rat hippocampus are associated with an inhibition of mitogen-activated protein kinase ERK. J. Neurochem. *75*, 634–643.

Teplow, D.B. (2006). Preparation of amyloid beta-protein for structural and functional studies. Methods Enzymol. *413*, 20–33.

Tran, M.H., Yamada, K., Olariu, A., Mizuno, M., Ren, X.H., and Nabeshima, T. (2001). Amyloid beta-peptide induces nitric oxide production in rat hippocampus: association with cholinergic dysfunction and amelioration by inducible nitric oxide synthase inhibitors. FASEB J. *15*, 1407–1409.

Vodovotz, Y., Lucia, M.S., Flanders, K.C., Chesler, L., Xie, Q.W., Smith, T.W., Weidner, J., Mumford, R., Webber, R., Nathan, C., et al. (1996). Inducible nitric oxide synthase in tangle-bearing neurons of patients with Alzheimer's disease. J. Exp. Med. *184*, 1425–1433.

Wahle, T., Thal, D.R., Sastre, M., Rentmeister, A., Bogdanovic, N., Famulok, M., Heneka, M.T., and Walter, J. (2006). GGA1 is expressed in the human brain and affects the generation of amyloid beta-peptide. J. Neurosci. *26*, 12838–12846.

Wang, Q., Rowan, M.J., and Anwyl, R. (2004). Beta-amyloid-mediated inhibition of NMDA receptor-dependent long-term potentiation induction involves activation of microglia and stimulation of inducible nitric oxide synthase and superoxide. J. Neurosci. *24*, 6049–6056.

Wilcock, D.M., Lewis, M.R., Van Nostrand, W.E., Davis, J., Previti, M.L., Gharkholonarehe, N., Vitek, M.P., and Colton, C.A. (2008). Progression of amyloid pathology to Alzheimer's disease pathology in an amyloid precursor protein transgenic mouse model by removal of nitric oxide synthase 2. J. Neurosci. *28*, 1537–1545.